

# Beyond GEMM-Centric NPUs: Enabling Efficient Diffusion LLM Sampling

Binglei Lou<sup>1</sup>, Haoran Wu<sup>2</sup>, Yao Lai<sup>2</sup>, Jiayi Nie<sup>2</sup>, Can Xiao<sup>1</sup>, Xuan Guo<sup>1</sup>,  
Rika Antonova<sup>2</sup>, Robert Mullins<sup>2</sup>, and Aaron Zhao<sup>1</sup>

<sup>1</sup>Imperial College London, <sup>2</sup>University of Cambridge, UK

**Abstract**—Diffusion Large Language Models (dLLMs) introduce iterative denoising to enable parallel token generation, but their sampling phase displays fundamentally different characteristics compared to GEMM-centric transformer layers. Profiling on modern GPUs reveals that sampling can account for up to 70% of total model inference latency—primarily due to substantial memory loads and writes from vocabulary-wide logits, reduction-based token selection, and iterative masked updates. These processes demand large on-chip SRAM and involve irregular memory accesses that conventional NPUs struggle to handle efficiently. To address this, we identify a set of critical instructions that an NPU architecture must specifically optimize for dLLM sampling. Our design employs lightweight non-GEMM vector primitives, in-place memory reuse strategies, and a decoupled mixed-precision memory hierarchy. Together, these optimizations deliver up to a  $2.53\times$  speedup over the NVIDIA RTX A6000 GPU under an equivalent nm technology node. We also open-source our cycle-accurate simulation and post-synthesis RTL verification code, confirming functional equivalence with current dLLM PyTorch implementations.

## I. INTRODUCTION

Autoregressive (AR) large language models (LLMs) are fundamentally constrained by sequential token generation during decoding, resulting in memory-bound bottlenecks on high-throughput accelerators. Diffusion-based LLMs (dLLMs) [1] have recently emerged as a promising alternative by enabling parallel token denoising, thereby amortizing token dependencies and increasing parallelism. By jointly refining multiple tokens across iterative denoising steps, dLLMs increase the arithmetic intensity of the decoding phase and mitigate the memory-bandwidth limitations inherent in AR decoding.

However, this shift in generation paradigm introduces new systemic inefficiencies. Figure 1 reports the latency breakdown for two representative dLLMs, LLaDA-8B-Instruct and LLaDA-MoE-7B-A1B, evaluated using the dInfer framework [2] with optimized vLLM backends. Our empirical analysis shows that although the transformer-based denoising phase (model) accounts for the majority of floating-point operations, the subsequent sampling phase—which performs vocabulary-wide reductions, rank-based selection, and irregular memory access—constitutes a disproportionately large fraction of the end-to-end latency, reaching up to 71% under mixture-of-experts (MoE) and dual KV-cache configurations [3]. As the community adopts increasingly aggressive quantization (e.g., 4/8-bit weights and activations), the execution time of the model phase is expected to shrink further. Following Amdahl’s Law, the inefficient sampling

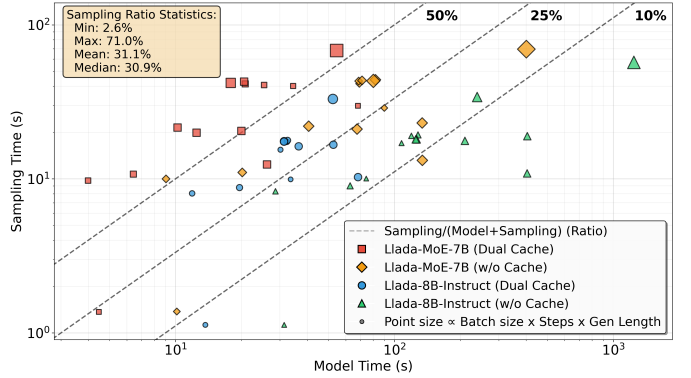


Fig. 1: Latency breakdown of the LLaDA model on an A6000 GPU, evaluated across a broad parameter space: batch sizes from 1 to 32, denoising steps from 1 to 32, generation lengths from 64 to 1024 tokens, and block sizes from 8 to 64.

stage thus becomes an inevitable long-tail bottleneck, limiting the throughput benefits of model-side optimization.

At each denoising iteration, the sampling stage materializes a logits tensor of dimension  $[B \times L \times V]$ , where  $B$  denotes the batch size,  $L$  is the block size, and  $V$  is the vocabulary size (reaching 120~160k in state-of-the-art dLLMs such as LLaDA [4] and DREAM [5]). Even a single batch with  $L = 64$  requires 16~19 MB under 16-bit floating-point representation. Multiple in-flight batches frequently exceed on-chip memory capacity, forcing off-chip transfers across DDR/HBM and exacerbating latency. While sampling quantization offers a promising orthogonal approach to reducing memory traffic, our work focuses on addressing the fundamental structural mismatch between the non-GEMM-centric sampling workload and the GEMM-centric execution pipelines in modern neural processing units (NPUs).

Contemporary NPU designs, exemplified by PLENA [6], are deeply optimized for dense matrix computations such as attention and MLP layers, yet provide limited support for the control-intensive, reduction-heavy, and memory-irregular operations required by diffusion sampling. As a result, sampling either incurs significant instruction overhead or offloads execution to host CPUs, degrading overall hardware efficiency and utilization [7–10].

To address these challenges, we propose d-PLENA, a vector-scalar-centric architectural extension that enables efficient on-NPU execution of dLLM sampling. Our contributions are as follows:

- 1) A hardware-friendly execution flow for softmax-based

diffusion sampling that enables in-place computation and phased memory reuse, while maintaining numerical equivalence to standard implementations.

- 2) We propose a set of lightweight non-GEMM ISA primitives to accelerate ArgMax, Top- $k$  selection, and masked token updates, which are essential for efficient diffusion sampling.
- 3) A decoupled mixed-precision memory hierarchy that separates floating-point and integer data domains, reducing memory fragmentation and control-path interference.
- 4) Comprehensive evaluation using a cycle-accurate simulator and post-synthesis RTL verification demonstrates numerical correctness and analyzes the impact of batch size, diffusion steps, and vocabulary size on sampling latency, on-chip SRAM utilization, HBM bandwidth, and overall hardware efficiency.

## II. BACKGROUND AND MOTIVATION

### A. PLENA Accelerator

PLENA [6] provides an end-to-end NPU development stack for Transformer-based LLM inference, including a custom ISA, compiler, cycle-accurate simulator, and automated design space exploration. Its ISA is designed for standard autoregressive transformer-based LLMs, such as Llama-3, and provides native support for GEMM-intensive layers, normalization, and FlashAttention [11]. The simulator models HBM-enabled memory systems using Ramulator [12], enabling detailed and realistic analysis of memory bandwidth, latency, and data movement for transformer inference workloads.

While PLENA is effective for conventional AR workloads, it does not explicitly expose architectural or toolchain support for patterns that arise in diffusion-based sampling.

### B. Diffusion-based LLMs and Blocked Sampling

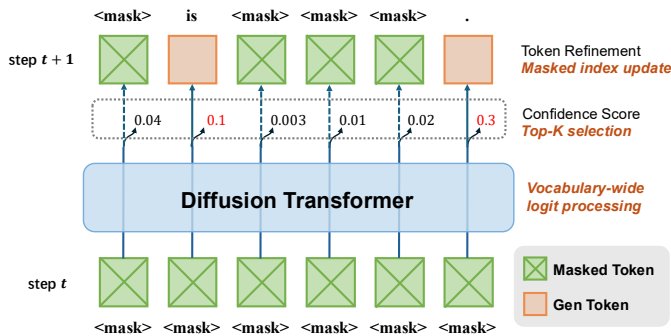


Fig. 2: Diffusion Large Language Model. For each timestep, the transformer predicts token confidences and updates the top- $k$  masked positions to progressively refine the sequence.

Diffusion LLMs, such as LLaDA [4], generate tokens through iterative denoising rather than strictly autoregressive (AR) decoding. At each diffusion step  $t$ , the model predicts vocabulary-wide logits for every token position, which are converted into a categorical distribution:

$$\mathbf{p}^{(t)} = \text{softmax}(\mathbf{z}^{(t)}), \quad \mathbf{z}^{(t)} \in \mathbb{R}^V, \quad (1)$$

where  $V$  denotes the vocabulary size.

For a batch of size  $B$  and a total generation length  $L_{\text{tot}}$ , a single diffusion step produces a logits tensor  $\mathbf{Z}^{(t)} \in \mathbb{R}^{B \times L_{\text{tot}} \times V}$ , which constitutes the dominant data structure during sampling. For each token position  $i$ , a scalar confidence score is computed from its corresponding vocabulary distribution  $\mathbf{p}_i^{(t)}$  (e.g., the maximum predicted probability). The Top- $k$  token positions with the highest confidence scores are then selected and unmasked, committing their predicted tokens, while the remaining positions stay masked and are refined in subsequent diffusion steps, as illustrated in Fig. 2.

Recent blocked dLLM approaches [3, 13] further improve efficiency by applying AR decoding across blocks while performing parallel diffusion within each block. Under this execution model, diffusion sampling at each step is restricted to an active block of tokens of block length  $L$ , operating on the corresponding subtensor  $\mathbf{Z}_{\text{active}}^{(t)} \in \mathbb{R}^{B \times L \times V}$ , while the remaining token positions are either already committed or deferred to subsequent blocks. Covering the full sequence thus involves iterating over  $L_{\text{tot}}/L$  blocks, with diffusion applied independently within each active block.

Although diffusion sampling algorithms continue to evolve, core operations such as vocabulary scanning, reduction, sorting, and masked selection remain largely invariant. This work targets these fundamental sampling primitives and maps them to hardware-efficient execution, as formalized in Algorithm 2.

## III. METHODOLOGY

### A. Proposed NPU Architecture

As illustrated in Fig. 3, the system adopts a multi-domain storage hierarchy to efficiently handle heterogeneous data types. Large-scale tensors, such as logits, are stored in HBM using the MX format. During sampling, these logits are streamed into the Vector SRAM through a dedicated Dequantizer, which converts MX-encoded data into a configurable floating-point format (e.g., BF16). To mitigate memory fragmentation and alignment overheads, the on-chip storage is decoupled into Vector, FP, and Int SRAM. In particular, the Int SRAM is physically isolated from the high-throughput vector data path and interfaces with the host via a FIFO buffer to deliver final token IDs with minimal control-path interference.

The execution core is composed of specialized compute units coordinated by an instruction decoder. The Vector Unit consists of two primary modules: a Reduction Unit and an Elementwise Unit. The Reduction Unit processes data in chunks of  $VLEN$  and supports operations such as Max and Sum, producing scalar outputs that are forwarded to the FP or Int Units. The Elementwise Unit preserves vector dimensionality and supports multi-operand vector operations. To accelerate non-linear sampling kernels, the FP Unit provides hardware-native support for transcendental functions, including  $e^x$  and  $1/x$ . These results can be directly broadcast back to the Vector Unit or buffered through the FP SRAM.

### B. Hardware-Friendly Sampling Flow

To streamline NPU execution, we reorganize the sampling flow into a hardware-friendly Stable-Max formulation, as

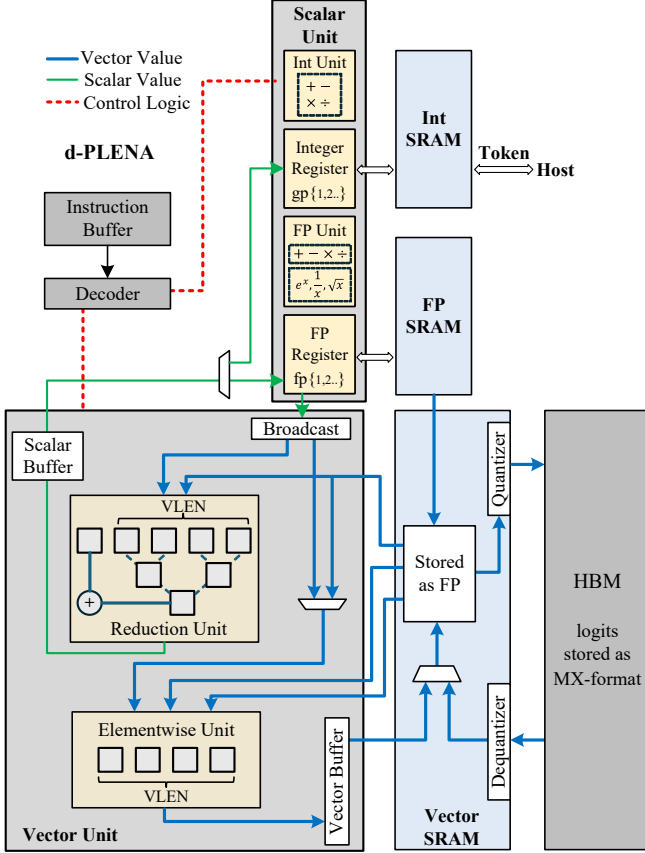


Fig. 3: Proposed NPU architecture for diffusion sampling.

illustrated in Algorithm 1. Unlike conventional softmax, which requires multiple memory passes and global normalization, the optimized Method 2 decomposes the computation into atomic primitives that map directly to dedicated hardware modules. Specifically, the Reduction Unit extracts the maximum value  $m$  and accumulates the sum of shifted exponentials  $sum\_exp$ , while the FP Unit evaluates the transcendental functions  $e^x$  and the reciprocal  $1/x$ . The intermediate  $exp\_shifted$  values are written back in-place, overwriting the original logits buffer in the Vector SRAM to maintain a high memory utilization.

#### Algorithm 1 Algorithmic Transformation: Software Softmax vs. Hardware-Friendly Stable-Max

```

1: METHOD 1: STANDARD SOFTMAX (PYTORCH-LIKE)
2:  $max\_idx \leftarrow \text{argmax}(logits)$ 
3:  $p \leftarrow \text{softmax}(logits)$ 
4:  $x_0\_p \leftarrow p[max\_idx]$ 
5: METHOD 2: STABLE-MAX (NPU-OPTIMIZED)
6:  $m \leftarrow \max(logits)$ 
7:  $exp\_shifted \leftarrow e^{logits - m}$ 
8:  $sum\_exp \leftarrow \sum exp\_shifted$ 
9:  $x_0\_p \leftarrow 1.0 / sum\_exp$ 

```

#### C. ISA Extensions for dLLM and Phased Sampling Execution

Table I summarizes the proposed ISA extensions, and Algorithm 2 outlines the high-level diffusion sampling flow adopted in LLaDA [4]. The temperature noise component based on the Gumbel-max trick is omitted for simplicity and

will be incorporated in future work. The Transformer-based dataflow is encapsulated in the `model()` operation, whose output logits serve as the input to the sampling stage. The `model()` is invoked at each diffusion time step  $t$ : at first  $t$ , the input is formed by a blocked slice of the concatenated prompt and mask tokens, and in subsequent steps, the updated token sequence  $x$  is fed back iteratively across  $T$  diffusion steps. The proposed ISA primitives are invoked within each iteration, in coordination with existing PLENA instructions [6]. We identify four hardware-visible execution phases in which the instructions listed in Table I are exercised.

#### Algorithm 2 Hardware-aware intra-block sampling for dLLMs

```

Require: model  $\triangleright$  LLM model before the diffusion denoising
Require: prompt  $\triangleright$  input to the dLLM
Require:  $T, B, L, V, V_{chunk}, R, VLEN$   $\triangleright$  diffusion steps, batch, generation length, vocabulary size, configurable chunk size†, iteration count  $R = V/V_{chunk}$ , vector processing unit
1:  $x \in \mathbb{R}^{B \times L} \leftarrow \text{blocked}[prompt, mask\_id]$ 
2:  $k \in \mathbb{R}^B \leftarrow \text{get\_num\_transfer\_tokens}(T)$ 
3: for  $t = 1$  to  $T$  do
4:    $logits \in \mathbb{R}^{B \times L \times V} \leftarrow \text{model}(x)$ 
5:    $m\_idx \in \mathbb{R}^{B \times L} \leftarrow (x == mask\_id)$ 
6:   for  $b = 1$  to  $B$  do
7:     for  $l = 1$  to  $L$  do
8:       PHASE 1  $\text{HBM} \rightarrow \text{VECTOR} \rightarrow \text{SCALAR}$ 
9:       for  $r = 1$  to  $R$  do
10:         †Preload  $V_{chunk}$  from HBM to Vector SRAM
11:         for  $i = 1$  to  $(V_{chunk}/VLEN)$  do
12:            $x_0\_p\_scalar \leftarrow \text{Alg. 1, Method 2 (logits)}$ 
13:            $x_0\_scalar \leftarrow \text{argmax}(logits)$ 
14:         end for
15:       end for
16:       PHASE 2  $\text{SCALAR}$ 
17:        $SRAM_{FP}[l] \leftarrow \text{fp\_reg}(x_0\_p\_scalar)$ 
18:        $SRAM_{INT}[l] \leftarrow \text{gp\_reg}(x_0\_scalar)$ 
19:     end for
20:     PHASE 3  $\text{SCALAR (FP)} \rightarrow \text{VECTOR} \rightarrow \text{SCALAR (INT)}$ 
21:      $x_0\_p \leftarrow \text{Map}(SRAM_{FP}[1 : L])$ 
22:      $transfer\_idx \leftarrow \text{Sort\_Top\_k}(x_0\_p, m\_idx, k)$ 
23:     PHASE 4  $\text{SCALAR (INT)}$ 
24:      $x_0 \leftarrow (SRAM_{INT}[1 : L])$ 
25:      $x_0 \leftarrow \text{torch.where}(m\_idx, x_0, x)$ 
26:      $x \leftarrow \text{torch.where}(transfer\_idx, x, x_0)$ 
27:   end for
28: end for
29: return  $x$ 

```

<sup>†</sup>  $V_{chunk}$  controls tiling: it enables chunked processing ( $V_{chunk} < V$ ) for SRAM-limited edge devices, or scales to  $B \times L \times V$  in resource-rich scenarios to maximize data reuse via outer-loop preloading.

**PHASE 1.** Logits are streamed from HBM into the Vector SRAM in parameterized chunks using PLENA’s `H_PREFETCH_V` instruction. In a streaming fashion, the confidence scalar  $x_0\_p\_scalar$  and the corresponding token index  $x_0\_scalar$  are computed via the Stable-Max reduction and the `V_RED_MAX_IDX` instruction, respectively. Notably, the `max()` and `argmax()` results can be achieved in a single instruction.

**PHASE 2.** The computed scalar confidence values and token indices are written back to the FP SRAM and Int SRAM, respectively, using the decoupled scalar store instructions `S_ST_FP` and `S_ST_INT`.

TABLE I: Summary of Custom ISA Instructions

Instruction (Format)	Description
V_RED_MAX_IDX (rd, rs1, rs2, rs3)	Vector reduction operation that finds the maximum value and its index.
S_ST_FP (rd, rs1, imm)	Store scalar floating-point value from FP register rd to FP SRAM.
S_ST_INT (rd, rs1, imm)	Store scalar integer value from GP register rd to INT SRAM.
S_MAP_V_FP (rd, rs1, imm)	Transfer $L$ FP-format elements from FP SRAM to Vector SRAM.
V_TOPK_MASK (rd, rs1, rs2, k_scalar)	Performs top- $k$ sorting.
V_SELECT_INT (rd, rs1, rs2, rs3)	Masked element-wise select operation on INT SRAM.

**PHASE 3.** Dense vectors are reconstructed from scalar entries in the Vector SRAM, after which a hardware-native Top- $k$  comparison generates a vectorized boolean transfer mask for candidate selection. This phase is implemented using S\_MAP\_V\_FP and V\_TOPK\_MASK. The vector processed here has  $L$  elements. We adopt a streaming insertion-based Top- $k$  architecture, which maintains a sorted list of the  $k$  largest values among the current sequence using  $k$  parallel comparators and shift registers. The hardware requires  $O(k)$  area and performs  $O(L \cdot k)$  comparison operations to maintain this operation.

**PHASE 4.** Masked token updates are applied in the integer domain. Guided by vector masks, the Int Unit performs parallel masked selection to update token indices directly. This operation is functionally equivalent to an element-wise `torch.where()` and is realized through the V\_SELECT\_INT instruction.

#### D. Co-design and Verification Framework

The hardware-software co-design framework is illustrated in Fig. 4. The front-end compiler facilitates the mapping of sampling logic from PyTorch configuration into the augmented d-PLENA ISA through automated scheduling and code generation. For architectural validation, the simulator-derived behavior is cross-verified against a PyTorch-based software reference for numerical accuracy. Finally, the design is implemented in RTL and processed through Synopsys synthesis tools to assess area and power overhead. This closed-loop framework ensures new architectural optimizations maintain high functional fidelity and predictable hardware performance.

## IV. EXPERIMENTAL RESULTS

### A. Experimental Setup

Functional evaluation is performed using a HBM-enabled (HBM2e) cycle-accurate simulator [12]. SystemVerilog RTL-level correctness is further verified using Cocotb-based simulation, while post-synthesis area and power results are obtained using Synopsys Design Compiler (DC) targeting a 7 nm OpenROAD design kit [14] under a 1 GHz clock frequency.

The following numerical formats are used throughout the evaluation: MX format: MXFP8 (E4M3), BF16 for FP-related computations and storing, INT32 for INT-related processing.

Section IV-B focuses on the edge scenario where on-chip SRAM capacity is limited. In this setting, we configure  $V_{\text{chunk}} < V$  (following Algorithm 2) and evaluate VLEN values of 64 and 128. The results show relatively high latency despite a small SRAM footprint (below 64 kB). In contrast, Section IV-C assumes that the entire logit tensor is preloaded into vector SRAM to eliminate the multiple times of data movements from HBM to SRAM.

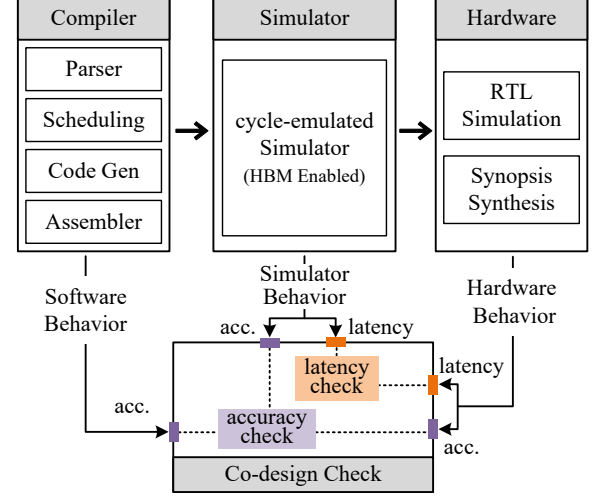


Fig. 4: Hardware-software co-design and verification workflow with cross-layer accuracy and latency checks.

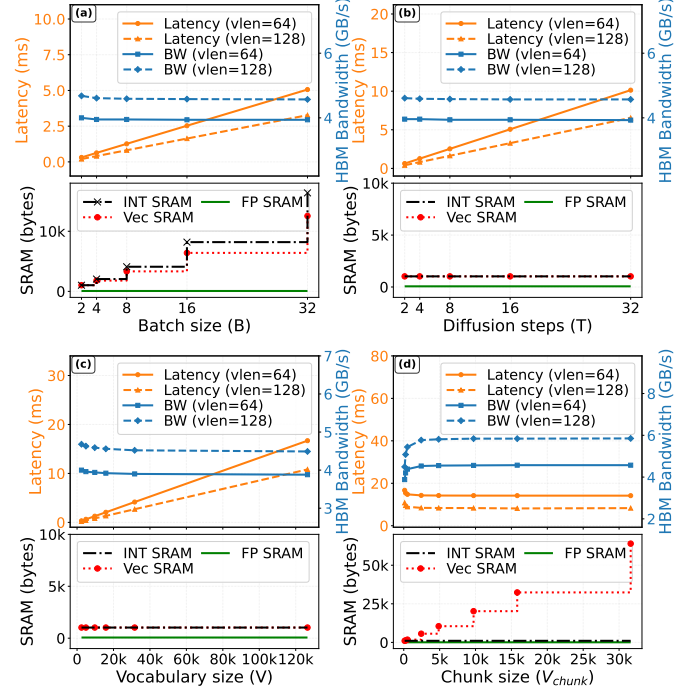


Fig. 5: Latency and Memory utilization of diffusion sampling.

### B. Latency and Memory Utilization

Figure 5 characterizes the performance of the proposed diffusion-sampling primitives under systematic sweeps of key workload parameters, with the `model()` execution excluded to isolate sampling overhead. All experiments fix the genera-

tion length to  $L = 64$ .

We first evaluate scalability with respect to batch size and diffusion steps by sweeping  $B, T \in \{2, 4, 8, 16, 32\}$  while fixing  $V = 2k$  and  $V_{chunk} = 128$ , as shown in Fig. 5(a) and (b), respectively. We then study the impact of vocabulary size by sweeping  $V$  from 2k to 128k under a fixed configuration of  $B = 2$ ,  $T = 1$ , and  $V_{chunk} = 128$ , as reported in Fig. 5(c). Finally, Fig. 5(d) examines the effect of chunk size  $V_{chunk}$  by sweeping it from 128 to 30k at the largest vocabulary setting ( $V = 128k$ ), with  $B = 2$  and  $T = 1$  fixed.

As shown in Fig. 5(a)–(c), the sampling latency scales approximately linearly with  $B$ ,  $T$ , and  $V$ , while the achieved HBM bandwidth remains nearly constant. This indicates stable bandwidth utilization and predictable performance scaling across these workload dimensions. In contrast, Fig. 5(d) shows that increasing the chunk size  $V_{chunk}$  reduces latency and improves effective HBM bandwidth by amortizing control and reduction overheads. Beyond approximately 4k entries, both metrics saturate, suggesting that large Vector SRAM capacities are not required to achieve near-peak efficiency, which is favorable for edge-oriented deployments.

The bottom inset of each sub-figure reports the on-chip SRAM footprint (in bytes) for the  $VLEN = 64$  configuration. The SRAM cost is evaluated as the number of elements determined by Eq. 2–Eq. 4, multiplied by their respective byte widths. For the vector SRAM,  $V_{chunk} < V$  corresponds to the edge mode, whereas in performance mode one can preload  $V \cdot L \cdot R$  elements from HBM into SRAM with  $R < B$  and  $R$  divisible by  $B$ . We report SRAM usage only for  $VLEN = 64$  because the Int SRAM and Vector SRAM footprints are invariant to  $VLEN$ , and the FP SRAM differs only by a small additive term proportional to  $VLEN$ . Under the proposed primitive design and across all parameter sweeps in the edge scenario, the on-chip SRAM footprint is dominated by the batch size  $B$  and  $V_{chunk}$ ; varying  $T$ ,  $V$ , or  $VLEN$  does not materially affect the overall requirement.

$$\text{Int elements} = 2 \cdot B \cdot L \quad (2)$$

$$\text{FP elements} = \max\{L, VLEN\} \quad (3)$$

$$\text{Vector elements} = \begin{cases} 3 \cdot B \cdot L + V_{chunk}, & \text{if } V_{chunk} < V, \\ 3 \cdot B \cdot L + V \cdot L \cdot R, & \text{otherwise} \end{cases} \quad (4)$$

### C. Execution Efficiency and Bottleneck Analysis

TABLE II: Sampling performance compared with GPU

Performance	A6000	d-PLENA(512)	d-PLENA(1024)	d-PLENA(2048)
Latency (ms)	2.51	3.41 (0.73 $\times$ )	1.79 (1.40 $\times$ )	0.99 (2.53 $\times$ )
Vector SRAM	-	8 MB	8 MB	8 MB
Int SRAM	-	8 kB	8 kB	8 kB
FP SRAM	-	1 kB	2 kB	4 kB

Table II compares GPU and d-PLENA performance on the same sampling workload with  $T = 1$ ,  $B = 16$ ,  $L = 32$ , and  $V = 126k$ . Here,  $R = 1$  is applied and indicates that single batches of the full block logits are preloaded into vector SRAM per iteration to balance the SRAM demand and HBM data transfers. With  $VLEN = \{512, 1024, 2048\}$ , the proposed NPU achieves a speedup up to 2.53 $\times$  over the NVIDIA RTX A6000.

TABLE III: Instruction-level latency breakdown

Category	Cycles	Ratio (%)
Vector	477,696	48.2%
Memory	392,320	39.6%
Scalar	117,412	11.8%
Other (control related)	3,609	0.4%
<b>Total</b>	<b>991,038</b>	<b>100.0%</b>

Table III further reveals the instruction-level breakdown of the largest test case (d-PLENA(2048)) in Table II. It shows that vector operations dominate the execution, accounting for 48.2% of the total cycles. Specifically, the hardware-accelerated reduction-sum (V\_RED\_SUM) and max-index (V\_RED\_MAX\_IDX) functions significantly compress the computation latency. Furthermore, the HBM prefetch logic (H\_PREFETCH\_V) sustains a high utilization of  $67.7 \times 10^9$  Bytes/sec, effectively feeding the vector units. The scalar and control overhead is kept below 12%, proving that our specialized ISA minimizes the scheduling overheads.

### D. Post-Synthesis Area and Power Evaluation

Finally, Post-synthesis results are reported in Table IV for multiple  $VLEN$  configurations. The synthesis results show that the area of the vector datapath scales approximately linearly with  $VLEN$ , whereas the scalar and control components remain largely insensitive to  $VLEN$ .

TABLE IV: Post-synthesis results for varying  $VLEN$ . The scalar area remains constant at  $661 \mu\text{m}^2$ .

$VLEN$	Vector Area ( $\mu\text{m}^2$ )	Total Power (mW)
512	0.731	381.72
1024	1.464	762.65
2048	2.931	1524.53

## V. CONCLUSION

As diffusion-based LLM adoption grows and model-side kernels get heavily optimized/quantized, the sampling tail threatens end-to-end latency. We analyzed these architectural challenges and proposed primitives are broadly suitable for reduction/selection-heavy workloads and could be exposed in future NPUs as standard features.

## REFERENCES

- [1] R. Yu, Q. Li, and X. Wang, “Discrete diffusion in large language and multimodal models: A survey,” *arXiv preprint arXiv:2506.13759*, 2025.
- [2] Y. Ma, L. Du, L. Wei, K. Chen, Q. Xu, K. Wang, G. Feng, G. Lu, L. Liu, X. Qi *et al.*, “diner: An efficient inference framework for diffusion language models,” *arXiv preprint arXiv:2510.08666*, 2025.
- [3] C. Wu, H. Zhang, S. Xue, Z. Liu, S. Diao, L. Zhu, P. Luo, S. Han, and E. Xie, “Fast-dilm: Training-free acceleration of diffusion lilm by enabling kv cache and parallel decoding,” *arXiv preprint arXiv:2505.22618*, 2025.
- [4] S. Nie, F. Zhu, Z. You, X. Zhang, J. Ou, J. Hu, J. Zhou, Y. Lin, J.-R. Wen, and C. Li, “Large language diffusion models,” *arXiv preprint arXiv:2502.09992*, 2025.
- [5] J. Ye, Z. Xie, L. Zheng, J. Gao, Z. Wu, X. Jiang, Z. Li, and L. Kong, “Dream 7b: Diffusion large language models,” *arXiv preprint arXiv:2508.15487*, 2025.
- [6] H. Wu, C. Xiao, J. Nie, X. Guo, B. Lou, J. T. Wong, Z. Mo, C. Zhang, P. Forsy, W. Luk *et al.*, “Combating the memory walls: Optimization pathways for long-context agentic lilm inference,” *arXiv preprint arXiv:2509.09505*, 2025.
- [7] S. Ghodrati, S. Kinzer, H. Xu, R. Mahapatra, Y. Kim, B. H. Ahn, D. K. Wang, L. Karthikeyan, A. Yazdanbakhsh, J. Park *et al.*, “Tandem processor: Grappling with emerging operators in neural networks,” in *Proceedings of the 29th ACM International Conference on Architectural Support for Programming Languages and Operating Systems, Volume 2*, 2024, pp. 1165–1182.
- [8] D. Xu, H. Zhang, L. Yang, R. Liu, G. Huang, M. Xu, and X. Liu, “Fast on-device lilm inference with npus,” in *Proceedings of the 30th ACM International Conference on Architectural Support for Programming Languages and Operating Systems, Volume 1*, 2025, pp. 445–462.
- [9] D. Xu, M. Xu, Q. Wang, S. Wang, Y. Ma, K. Huang, G. Huang, X. Jin, and X. Liu, “Mandhelng: Mixed-precision on-device dnn training with dsp offloading,” in *Proceedings of the 28th Annual International Conference on Mobile Computing And Networking*, 2022, pp. 214–227.
- [10] Z. Hao, J. Wei, T. Wang, M. Huang, H. Jiang, S. Jiang, T. Cao, and J. Ren, “Scaling lilm test-time compute with mobile npu on smartphones,” *arXiv preprint arXiv:2509.23324*, 2025.
- [11] T. Dao, “Flashattention-2: Faster attention with better parallelism and work partitioning,” *arXiv preprint arXiv:2307.08691*, 2023.
- [12] H. Luo, Y. C. Tuğrul, F. N. Bostancı, A. Olgun, A. G. Yağlıkçı, and O. Mutlu, “Ramulator 2.0: A modern, modular, and extensible dram simulator,” *IEEE Computer Architecture Letters*, vol. 23, no. 1, pp. 112–116, 2023.
- [13] M. Arriola, A. Gokaslan, J. T. Chiu, Z. Yang, Z. Qi, J. Han, S. S. Sahoo, and V. Kuleshov, “Block diffusion: Interpolating between autoregressive and diffusion language models,” *arXiv preprint arXiv:2503.09573*, 2025.
- [14] L. T. Clark, V. Vashishtha, L. Shifren, A. Gujja, S. Sinha, B. Cline, C. Ramamurthy, and G. Yeric, “Asap7: A 7-nm finfet predictive process design kit,” *Microelectronics Journal*, vol. 53, pp. 105–115, 2016.